http://dx.doi.org/10.5012/bkcs.2012.33.9.3033

Investigation of the Hydrogen Storage Mechanism of Expanded Graphite by Measuring Electrical Resistance Changes

Ji Sun Im, Seung Soon Jang,[†] and Young-Seak Lee[‡,*]

Institute for Superconducting and Electronic Materials (ISEM), University of Wollongong, Wollongong, New South Wales 2522, Australia
[†]School of Materials Science and Engineering, Georgia Institute of Technology, 771 Ferst Drive NW, Atlanta, GA 30332-0245, USA
[‡]Department of Fine Chemical Engineering and Applied Chemistry, BK21-E[2]M, Chungnam National University, Daejeon 305-764, Korea. [*]E-mail: youngslee@cnu.ac.kr
Received May 8, 2012, Accepted June 25, 2012

The hydrogen storage mechanism of graphite was studied by measuring the electrical resistance change. Graphite was expanded and activated to allow for an easy hydrogen molecule approach and to enlarge the adsorption sites. A vanadium catalyst was simultaneously introduced on the graphite during the activation process. The hydrogen storage increased due to the effects of expansion, activation, and the catalyst. In addition, the electrical resistance of the prepared samples was measured during hydrogen molecule adsorption to investigate the hydrogen adsorption mechanism. It was found that the electrical resistance changed as a result of the easy hydrogen molecule approach, as well as of the adsorption process and the catalyst. It was also notable that the catalyst improved not only the hydrogen storage capacity but also the speed of hydrogen storage based on the response time. The hydrogen storage mechanism is suggested based on the effects of expansion, activation, and the catalyst.

Key Words : Hydrogen storage, Mechanism, Electrical resistance, Graphite, Catalyst

Introduction

Alternative energy is becoming essential because fossil fuels will be depleted within a few decades. There are a variety of alternative energies, such as geothermal, nuclear, wind, solar, and hydrogen. Hydrogen is a promising energy resource due to its unlimited supply, clean energy cycle system, and high efficiency. One of the challenges in using hydrogen energy is the lack of an efficient hydrogen storage media. Generally, there are three methods for hydrogen storage: high-pressure systems, cryogenic systems, and storage media. High-pressure systems have a risk of leakage even if special cylinders are used, and cryogenic systems are costly because they must be kept at a low temperature. Therefore, many researchers have tried to find a media for efficiently storing hydrogen energy.[1-5]

Activated carbon has been investigated as a hydrogen storage media because it has a high specific surface area and pore volume for hydrogen uptake. Researchers reported that expanded graphite can provide space among its layers for hydrogen molecule adsorption; therefore, graphite has been considered for hydrogen storage. There are two important ways to improve the amount of hydrogen that can be stored using carbon materials. The first is to control the pore size for optimum hydrogen molecule adsorption (a micropore size of approximately 0.7 nm is optimal). The other way is to use a catalyst to increase the efficiency of hydrogen adsorption. It has been reported that transition metal catalysts can improve hydrogen adsorption by the dissociation of hydrogen molecules and the adsorption of hydrogen in the pores of carbon materials. Therefore, various transition metal catalysts have been investigated.[6-10]

The mechanism for hydrogen storage is still not fully understood. Here, we investigate the mechanism based on the electrical resistance change of carbon materials during hydrogen molecule adsorption. In this study, graphite was expanded to enlarge the distance between graphite layers for hydrogen adsorption (presented in Scheme 1(a) and (b)). Next, the activation process was carried out to provide a high specific surface area and pore volume for hydrogen storage (presented in Scheme 1(c)). During this activation process, the transition metal catalyst was introduced into the carbon materials (presented in Scheme 1(d)). The mechanism of hydrogen storage was studied by measuring the electrical resistance change during hydrogen molecule adsorption. The hydrogen storage mechanism is discussed based on the effects of surface area, pore volume, pore size, and the catalyst.

Experimental

Preparation of Expanded Graphite. Graphite oxide was prepared using the Hummers method.[11] Graphite flakes (Sigma-Aldrich), sulfuric acid, potassium permanganate, sodium nitrate, and hydrogen peroxide were purchased for the preparation of graphite oxide. Expanded graphite was prepared using urea as an expansion-reduction agent, as in referenced article.[12] Specifically, the mixture of graphite oxide

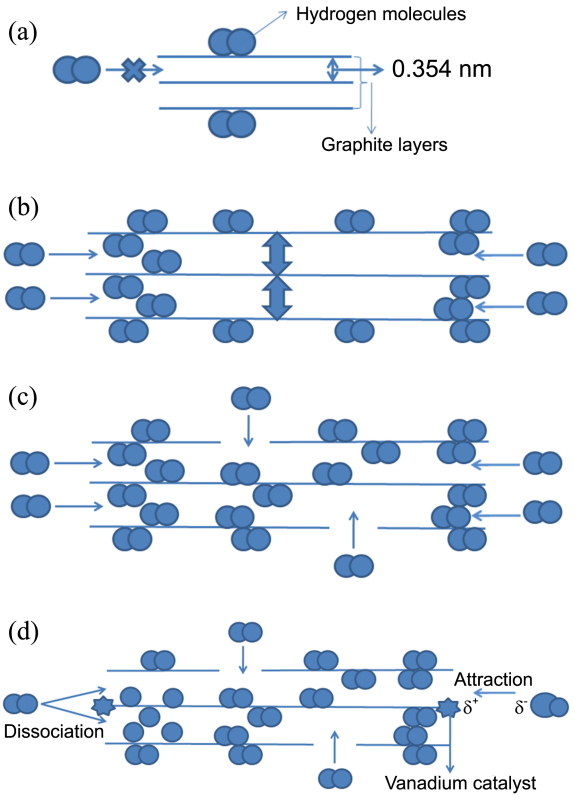

Scheme 1. Suggested hydrogen storage mechanism: (a) Raw graphite, (b) Expansion effect, (c) activation effect, and (d) catalyst effect.

and urea was prepared in a 1:1 molar ratio by grounding. The mixture was thermally treated at 600 °C with a nitrogen gas flow of 120 sccm by considering the urea decomposition temperature (below 600 °C).

Activation Process and Vanadium Catalyst Introduction. Four potassium hydroxide (KOH) solutions (2, 4, 6, and 8 M, 20 mL) were prepared as chemical activation agents to study the role of chemical agent. Various amounts (1, 2, and 3 g) of vanadium oxide (V_2O_5) were dissolved in the prepared 8 M KOH solutions to investigate the role of vanadium catalyst. Seven solutions were prepared in total for chemical activation and catalyst introduction. The prepared expanded graphite was placed on an alumina boat in a steel pipe at a ratio of 15 mL/g (each prepared solution/expanded graphite) for chemical activation. Activation was conducted at 700 °C for 1 h in an argon atmosphere. The heating rate was 5 °C/min, and the feed rate of the argon gas was 50 mL/min. After chemical activation, the resultant samples were washed with distilled water several times to remove residual potassium and then dried overnight at 150 °C.[13-17] These activated samples were labeled RG (raw graphite), EG (expanded graphite), A2-EG, A4-EG, A6-EG, and A8-EG (activated EG in 2, 4, 6 or 8 M KOH solution, respectively). CA8-EG series (catalyst introduced in A8-EG) were named C1A8-EG, C2A8-EG, and C3A8-EG according to the amount (1, 2, or 3 g) of vanadium oxide used.

Measurement of Hydrogen Storage Capacity. The hydrogen adsorption was carried out at 25 °C in pressure range of 1.77×10^{-1} Pa - 10 MPa. The details are provided in our previous works.[18-20]

Eq. (1) was used to calculate the hydrogen uptake capacity:

$$\text{Hydrogen storage efficiency} = (W_H/W_S) \times 100 \text{ (wt \%)} \quad (1)$$

where W_H is the weight of adsorbed hydrogen molecules and W_S is the weighted sum of the loaded samples and adsorbed hydrogen molecules during the hydrogen adsorption measurement. This measurement was carried out five times for each sample to study the recycling capacity.

Measurement of Electrical Resistance During Hydrogen Adsorption on a Prepared Sample. The hydrogen storage behavior was investigated by electrical resistance measurement using a programmable electrometer (Keithley 6514) during the hydrogen molecule adsorption on the prepared sample. The electrical resistance was initially measured in vacuum to stabilize the electrical resistance (until there was no change in electrical resistance). Hydrogen gas was injected to the sensor chamber (1500 cm^3) at a rate of 100 sccm while measuring the electrical resistance.

Sample Characterization. Morphological changes in the graphite structure were investigated using a field emission transmission electron microscope (FE-TEM, JEM-2100F HR). Structural changes in the graphite were investigated by focusing on the orientation of the carbon structures and the presence of defects from the expansion and activation treatments. Raman analysis was carried out to determine the I_g/I_d (intensity of graphite/intensity of defects) ratio of the graphite. Raman spectral analysis was conducted with an excitation power of 10 mW at a 514-nm wavelength using a RM 1000-In*Via* instrument (Renishaw).

Nitrogen adsorption was conducted on prepared samples at −196 °C using a surface analyzer (Micromeritics ASAP 2020) to measure textural properties, such as the specific surface area, the total pore volume and the micropore volume.

The X-ray photoelectron spectroscopy (XPS) spectra of the samples were obtained using a MultiLab 2000 spectrometer (Thermo Electron Co., Al Kα X-ray source, 0.5-eV step size) to study the introduced vanadium catalyst.

Results

The Hummers method for graphite oxide (GO) and the urea-induced method for EG (or for graphene) have been widely used; therefore, we focused on the effects of developed pore structure and the introduced vanadium catalyst based on the hydrogen adsorption behavior. The general characteristics of GO and EG were presented in previous works.[11,12]

Surface Morphologies and Pore Structures of Prepared Samples. The surface morphologies of RG and EG samples are shown in the TEM images of Figure 1. RG samples exhibited many dense areas that were attributed to a multi-layered structure, whereas EG samples exhibited thinner layers. Therefore, the treatments in this study expanded the

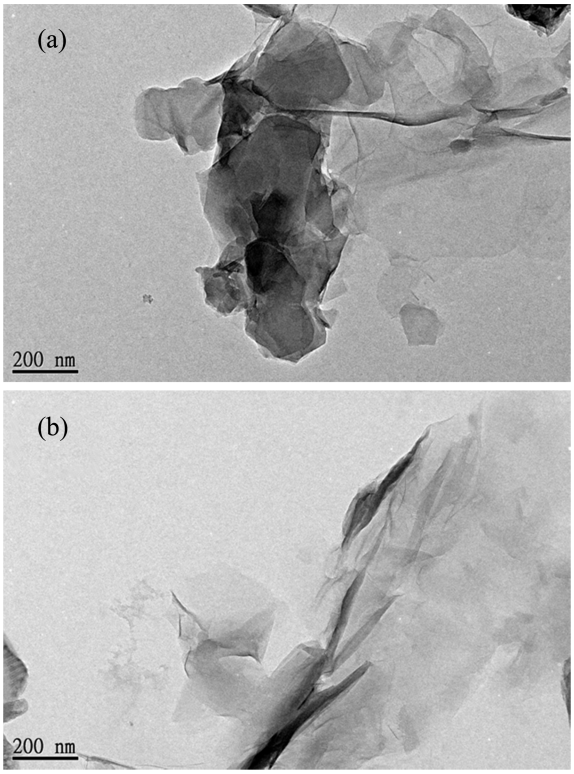

Figure 1. Surface morphologies of (a) RG and (b) EG.

graphite.

The textural properties of the prepared samples are summarized in Table 1. The pore structure of the graphite was developed by expansion and activation processes, resulting in an increased SSA (specific surface area) and TPV (total pore volume). Even though the SSA and TPV were increased by expansion, the pore structure developed mainly *via* the activation process, which yielded maximum SSA and TPV values of 345 m^2/g and 0.126 cm^3/g, respectively. The SSA and TPV were decreased slightly due to the combination effects of heavy weight and blocked some pores caused by introduced vanadium catalyst. It is not feasible to measure pore structures that are smaller than 1 nm using nitrogen molecule adsorption at 77 K[21,22]; therefore, it is not accurate to interpret the micro-structure based on the micropore volume (MPV) measured using nitrogen adsorption. Therefore, MPV is used as a reference measure to assess the effects of expansion and activation on the micropore structure. As listed, the MPV was also increased by expansion and activation, with the exception of sample A8-EG. A more interesting trend is that the micropores were primarily generated with a relatively small amount of KOH (the MPV percentage of A2-EG was approximately 70%), whereas the mesopore structure was developed with a relatively large amount of KOH (the MPV percentage of A8-EG was approximately 34%). This result can be attributed to the effect that micropores have on mesopore formation. In addition, the MPV was increased by the loaded vanadium catalyst because small mesopores were changed into micropores through a special reduction process. It is well known that micropore structures are beneficial for advanced hydrogen storage[18,19,23-25]; therefore, one can expect hydrogen storage to improve with an enlarged pore structure and controlled pore size.

Graphite Structure and Elemental Composition. Figure 2 presents the Raman spectra of the RG, EG, and A8-EG samples to illustrate the defects and graphite structures resulting from the expansion and activation of graphite. RG (the original graphite powder) exhibits two Raman modes at 1580 (G band, E_{2g2} symmetry, explained by the high crystalline quality of graphite lattice) and 1360 cm^{-1} (D band, A_{1g} symmetry, explained by double resonance process including an elastic scattering due to a defect). [26] As seen in Figure 1, the intensity of the G band (I_g) decreased and the intensity of the D band (I_d) increased simultaneously. The I_g/I_d ratios of RG, EG, and A8-EG were 11.95, 6.86, and 2.21, respectively. The obtained Raman results match the Tuinstra and Koening modeling indicating the structural change from graphite to nano crystalline graphite.[27-29] Therefore, we conclude that the graphite structure was crushed to a nanocrystalline graphite structure, but it still had a graphite structure. The amount of loaded vanadium was studied using the XPS elemental survey curve in Figure 3. The C1s peak was a dominant peak indicating that most elements were carbon. The V2p peak increased as the use of vanadium oxide

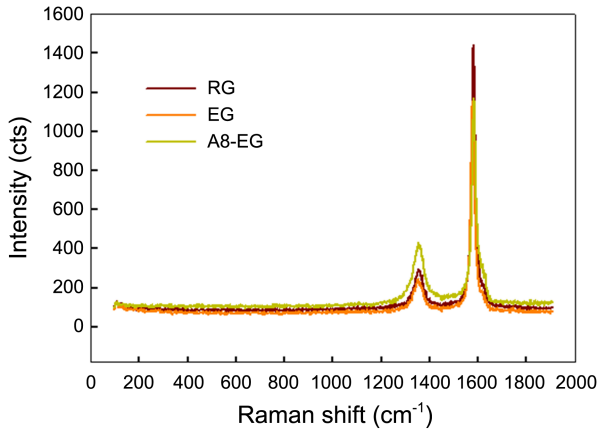

Figure 2. Raman data for the RG, EG and A8-EG samples.

Table 1. Textural properties of the prepared samples

	RG	EG	A2-EG	A4-EG	A6-EG	A8-EG	C1A8-EG	C2A8-EG	C3A8-EG
[a]SSA (m^2/g)	4.5	65	184	244	296	345	322	301	268
[b]TPV (cm^3/g)	-	0.028	0.062	0.079	0.102	0.126	0.119	0.104	0.098
[c]MPV (cm^3/g)	-	0.016	0.043	0.045	0.048	0.043	0.048	0.051	0.052

[a]SSA: specific surface area, [b]TPV: total pore volume, and [c]MPV: micropore volume

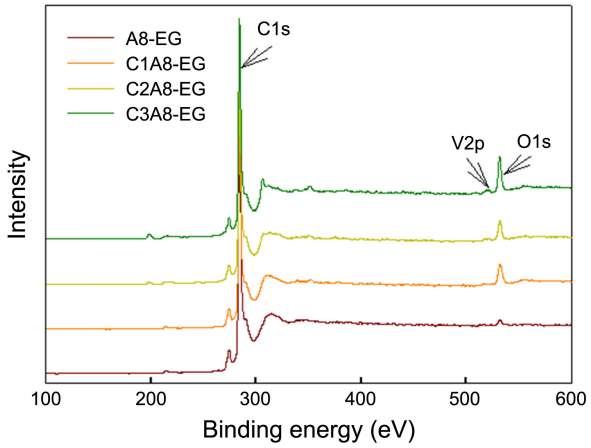

Figure 3. Elemental survey curve of the vanadium-loaded samples.

Table 2. Elemental composition summary of the vanadium-loaded samples

Atomic %	A8-EG	C1A8-EG	C2A8-EG	C3A8-EG
C	96.2	90.3	87.2	84.2
O	3.8	8.1	7.5	9.1
V	-	1.6	5.3	6.7

(vanadium catalyst source) increased. Details regarding elemental compositions are provided in Table 2.

Hydrogen Storage Behaviors of Developed Pore Structures with an Introduced Vanadium Catalyst. Hydrogen storage behaviors were investigated based on the effects of the developed pore structure and the introduced vanadium catalyst (presented in Figure 4). The RG sample stored the least amount of hydrogen because the typical distance between the graphite layers is 0.3354 nm.[30,31] Given the dynamic hydrogen molecule size, this distance is not sufficient for hydrogen adsorption. The amount of hydrogen stored in the EG sample reached 0.57 wt %. This result is attributed to the expanded space between the graphite layers. This also resulted in a developed pore structure with an enlarged SSA and TPV. The hydrogen molecules were adsorbed more effectively in the activated samples because activated samples can provide more sites for hydrogen storage due to the

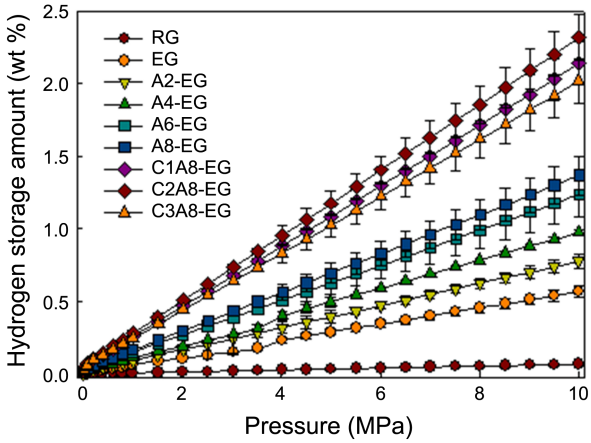

Figure 4. Hydrogen storage measured at 25 °C and 10 MPa.

developed pore structure. The amount of stored hydrogen increased gradually as a greater amount of KOH was used. This led to a substantially improved pore structure. Eventually, the A8-EG sample demonstrated a hydrogen uptake of 1.37 wt %. The amount of hydrogen stored by the activated samples (A2-EG, A4-EG, A6-EG, and A8-EG) suggests that hydrogen molecule adsorption occurred more effectively in micropores than mesopores. The gap in the hydrogen storage amount is relatively low, especially when comparing the A6-EG and A8-EG samples. This is because the micropore fraction for these samples is lower than that of other samples due to the micropore merging effects that are previously explained by BET analysis. The C1A8-EG, C2A8-EG, and C3A8-EG samples demonstrate that the vanadium catalyst improved the hydrogen storage capability. Briefly, there are two ways to explain the mechanism by which a metal catalyst can improve hydrogen storage. First, it is well known that transition metal catalysts can dissociate hydrogen molecules. Furthermore, dissociated hydrogen molecules can be stored in the pores of carbon materials. Thus, this suggested mechanism is called the spill-over phenomenon.[32-34] The other suggested mechanism is that the introduced metal can attract the hydrogen molecules by dipole-induced effects because metal catalysts have a δ^+ electron charge.[22,35] Specifically, the hydrogen molecules will have dipolar electron attraction effects on the metal catalyst, which encourages hydrogen adsorption. We believe that both of these mechanisms can occur during hydrogen adsorption, leading to a synergistic effect. Eventually, the hydrogen storage amount reached 2.32 wt % due to the improved pore structure, controlled pore size, and metal catalyst. The reason for the reduced hydrogen storage in the C3A8-EG sample is the decrease in pore structure by steric obstruction due to excessive amounts of the metal catalyst.

Discussion

Electrical Resistance Changes During Hydrogen Adsorption. The hydrogen molecule adsorption behaviors of the three samples (RG, A8-EG, and C2A8-EG) were discussed by electrical resistance changes during hydrogen adsorption (presented in Figure 5). The RG sample acted as a typical p-type semiconductor by enabling electron transport from hydrogen atoms (electron-donating) to the RG sample. The hole carriers were annihilated by transferred electrons, demonstrating increased electrical resistance.[36] The electrical resistance of RG increased gradually by up to 2.7% at approximately 13 min and then maintained.

The activated A8-EG samples exhibited the opposite trend, indicating that they lost their semiconductor characteristics because of the destroyed π-bonds in the graphite structure. The gas-sensing properties of porous carbon do not follow the characteristics of a semiconductor because the hexagonal carbon ring structure in graphite is largely destroyed.[37] The electrical resistance of porous carbon decreases the electron-hopping effects due to gas adsorption in pores.[37,38] Therefore, the A8-EG sample showed reduced electrical resistance.

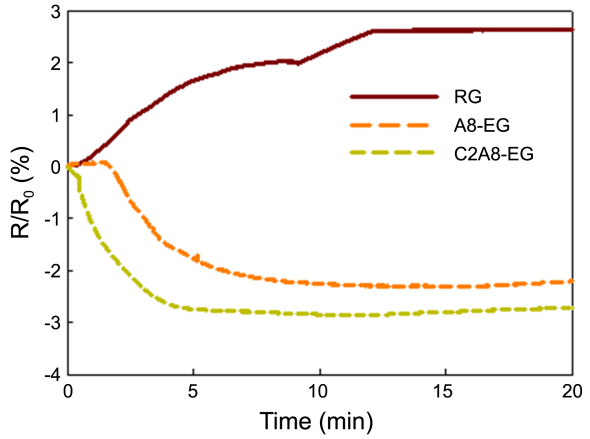

Figure 5. Electrical resistance measurements of the prepared samples during hydrogen adsorption.

The electrical resistance was decreased more strikingly by the vanadium catalyst. The electrical responsiveness for hydrogen adsorption was enhanced in C2A8-EG sample, and the response was achieved more quickly. The improved responsiveness to the presence of hydrogen can be attributed to the effect of the vanadium catalyst, which promotes hydrogen storage. Based on the quicker response time, it was found that the vanadium catalyst improves not only the hydrogen storage capacity but also the speed of hydrogen storage. This observation is difficult to reconcile with typical hydrogen storage measurements, such as those obtained using volumetric and gravimetric methods, because each data point requires too much time to obtain due to slow stabilization.

Suggested Mechanism of Hydrogen Storage for Modified Graphite Samples. The hydrogen storage mechanism of the prepared samples was discussed by assessing the effects of expansion, activation, and catalyst load on graphite. Scheme 1(a) shows the depicted hydrogen adsorption on RG. The optimum pore diameter/width is about 0.7 nm, as predicted by Monte-Carlo simulations.[23-25] Therefore, it is easy to predict that hydrogen adsorption is feasible only on the surface of graphite and not in the layers between the graphite sheets. Thus, it is necessary to expand the width between the graphite layers. The effect of graphite expansion on hydrogen adsorption is presented in Scheme 1(b). Hydrogen molecules can access the slip pores in the expanded graphite because of the increased width. In spite of increased width of graphite, there is a steric interference in hydrogen storage because the hydrogen molecules can more feasibly access the edge of EG than the middle of EG due to the large aspect ratio from graphite intrinsic property. Therefore, the pathway in the middle of the graphite will be valuable for hydrogen storage. The activation effect of EG is presented in Scheme 1(c). Hydrogen molecules are saved even in the middle of graphite through a pathway built by chemical activation. The catalyst effect is explained in Scheme 1(d). We developed two general explanations regarding the effect of the catalyst. One potential explanation is that hydrogen storage might increase *via* the spill-over phenomenon. Specifically, hydrogen molecules are dissociated on the surface of the introduced transition metal (here, vanadium) catalyst, as depicted on the left side of Scheme 1(d). The other potential explanation is that the hydrogen molecules are attracted into the graphite pores due to formed dipoles in hydrogen molecules. Even though the role of metal catalysts in hydrogen storage remains unclear, we think that the two suggested mechanisms can occur simultaneously. We can also provide a useful explanation for the role of the catalyst based on the electrical resistance measurements of the prepared samples during hydrogen storage. As discussed in hydrogen storage result, the metal catalyst both increases and quickens hydrogen storage. Therefore, the increased hydrogen storage is derived from improved physical hydrogen adsorption by the expansion and activation of graphite, as well as from the introduced metal catalyst by encouraging hydrogen adsorption *via* a chemical reaction (from either the spill-over phenomenon or electrical attraction). In summary, hydrogen storage using graphite was effectively improved by expansion, activation, and the use of a catalyst.

Conclusions

Hydrogen storage media was prepared by expanding and activating graphite. A vanadium catalyst was also introduced on the graphite to increase the hydrogen adsorption efficiency. The extended distance between the graphite layers allowed for an easy hydrogen molecule approach, and the enlarged surface area due to activation resulted in high hydrogen uptake *via* the availability of a sufficient number of adsorption sties. In addition, the investigation of the electrical resistance change in samples during hydrogen adsorption revealed that the vanadium catalyst both increases and quickens hydrogen storage. In conclusion, the hydrogen storage mechanism was studied based on its facilitation of an easy hydrogen molecule approach, and efficient hydrogen storage was achieved by expansion, activation, and the use of a metal catalyst.

Acknowledgments. This work was supported by the National Research Foundation of Korea Grant funded by the Korean Government MEST, Basic Research Promotion Fund (NRF-2011-013-D00031).

References

1. Hardy, B.; Corgnale, C.; Chahine, R.; Richard, M. A.; Garrison, S.; Tamburello, D.; Cossement, D.; Anton, D. *Int. J. Hydrogen Energ.* **2012**, *37*, 5691.
2. Chen, C. Y.; Chang, J. K.; Tsai, W. T. *Int. J. Hydrogen Energ.* **2012**, *37*, 3305.
3. Yoo, H. M.; Lee, S. Y.; Kim, B. J.; Park, S. J. *Carbon Lett.* **2011**, *12*, 112.
4. Bai, B. C.; Kim, J. G.; Naik, M.; Im, J. S.; Lee, Y. S. *Carbon Lett.* **2011**, *12*, 171.
5. Yang, S. J.; Jung, H.; Kim, T.; Im, J. H.; Park, C. R. *Int. J. Hydrogen Energ.* **2012**, *37*, 5777.
6. Sayed Ahmed, S. A.; Abo El-enin, R. M. M.; El-Nabarawy, Th.

Carbon Lett. **2011**, *12*, 152.
7. Manocha, S.; Brahmbhatt, A. *Carbon Lett.* **2011**, *12*, 85.
8. Bai, B. C.; Kim, J. G.; Im, J. S.; Jung, S. C.; Lee, Y. S. *Carbon Lett.* **2011**, *12*, 236.
9. Jiménez, V.; Ramírez-Lucas, A.; Sánchez, P.; Valverde, J. L.; Romero, A. *Int. J. Hydrogen Energ.* **2012**, *37*, 4144.
10. Singh, P.; Kulkarni, M. V.; Gokhale, S. P.; Chikkali, S. H.; Kulkarni, C. V. *Appl. Surf. Sci.* **2012**, *258*, 3405.
11. Hummers, W. S., Jr.; Offeman, R. E. *J. Am. Chem. Soc.* **1958**, *80*, 1339.
12. Wakeland, S.; Martinez, R.; Grey, J. K.; Luhrs, C. C. *Carbon* **2010**, *48*, 3463.
13. Ruth, U. P.; Francisco, C. M.; David, F. J.; Carlos, M. C. *Micropor. Mesopor Mat.* **2006**, *92*, 64.
14. Górka, J.; Zawislak, A.; Choma, J.; Jaroniec, M. *Appl. Surf. Sci.* **2010**, *256*, 5187.
15. Castro, M. M.; Manuel, M. E.; Miguel, M. S.; Francisco, R. R. *Carbon* **2010**, *48*, 636.
16. Im, J. S.; Park, S. J.; Kim, T. J.; Kim, Y. H.; Lee, Y. S. *J. Colloid Interf. Sci.* **2008**, *318*, 42.
17. Armandi, M.; Bonelli, B.; Geobaldo, F.; Garrone, E. *Micropor. Mesopor Mat.* **2010**, *132*, 414.
18. Im, J. S.; Kwon, O.; Kim, Y. H.; Park, S. J.; Lee, Y. S. *Micropor. Mesopor Mat.* **2008**, *115*, 514.
19. Im, J. S.; Park, S. J.; Lee, Y. S. *Mater. Res. Bull.* **2009**, *44*, 1871.
20. Im, J. S.; Kang, S. C.; Bai, B. C.; Suh, J. K.; Lee, Y. S. *Int. J. Hydrogen Energ.* **2011**, *36*, 1560.
21. Kim, B. J.; Lee, Y. S.; Park, S. J. *Int. J. Hydrogen Energ.* **2008**, *33*, 2254.
22. Kim, B. J.; Park, S. J. *Int. J. Hydrogen Energ.* **2011**, *36*, 648.
23. Kuchta, B.; Firlej, L.; Roszak, S.; Pfeifer, P. *Adsorption* **2010**, *16*, 413.
24. Zubkov, V. V.; Samsonov, V. M.; Grinev, I. V. *J. Surf. Invest.* **2012**, *6*, 49.
25. Fomkin, A. A.; Sinitsyn, V. A. *Russ. Chem. Bull.* **2009**, *58*, 706.
26. Pócsik, I.; Hundhausen, M.; Koós, M.; Ley, L. *J. Non-Cryst. Solids* **1998**, *227-230*, 1083.
27. Tuinstra, F.; Koenig, J. L. *J. Chem. Phys.* **1970**, *53*, 1126.
28. Ferrari, A. C.; Robertson, J. *Phys. Rev. B* **2000**, *61*, 14095.
29. Lee, H.; Kim, I. Y.; Han, S. S.; Bae, B. S.; Choi, M. K.; Yang, I. S. *J. Appl. Phys.* **2001**, *90*, 813.
30. Gupta, V.; Nakajima, T.; Ohzawa, Y.; Žemva, B. *J. Fluorine Chem.* **2003**, *120*, 143.
31. Gupta, V.; Nakajima, T.; Zemva, B. *J. Fluorine Chem.* **2001**, *110*, 145.
32. Lueking, A.; Yang, R. T. *J. Catal.* **2002**, *206*, 165.
33. Chen, C. H.; Huang, C. C. *Micropor. Mesopor Mat.* **2008**, *109*, 549.
34. Lueking, A. D.; Yang, R. T. *Appl. Catal.* **2004**, *A 265*, 259.
35. Im, J. S.; Park, S. J.; Lee, Y. S. *Int. J. Hydrogen Energ.* **2009**, *34*, 1423.
36. Li, W.; Hoa, N. D.; Kim, D. *Sens. Actuator B-Chem.* **2010**, *149*, 184.
37. Im, J. S.; Kang, S. C.; Bai, B. C.; Bae, T. S.; In, S. J.; Jeong, E.; Lee, Y. S. *Carbon* **2011**, *49*, 2235.
38. Im, J. S.; Kang, S. C.; Lee, S. H.; Lee, Y. S. *Carbon* **2010**, *48*, 2573.